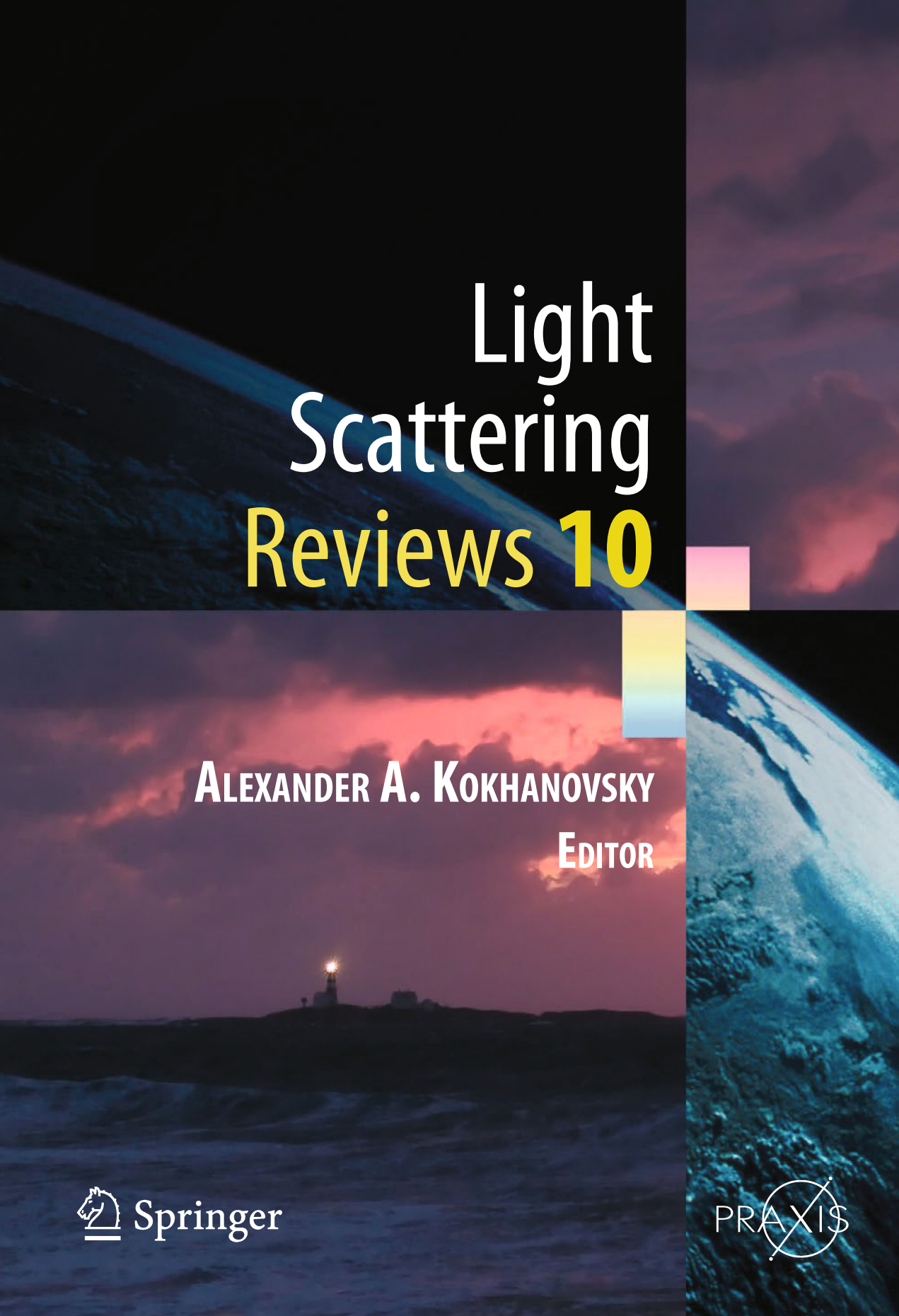
Light
Scattering
Reviews 10
Alexander A. Kokhanovsky
Editor
Springer
PRAXIS

Light Scattering Reviews 10

Light Scattering and Radiative Transfer

Alexander A. Kokhanovsky (Editor)

Light Scattering Reviews 10

Light Scattering and Radiative Transfer

Published in association with
Praxis Publishing
Chichester, UK

Editor
Dr. Alexander A. Kokhanovsky
EUMETSAT
Darmstadt, Germany

SPRINGER–PRAXIS BOOKS IN ENVIRONMENTAL SCIENCES (*LIGHT SCATTERING SUB-SERIES*)
EDITORIAL *ADVISORY BOARD MEMBER*: Dr. Alexander A. Kokhanovsky, Ph.D., Institute of Environmental Physics, University of Bremen, Bremen, Germany

ISBN 978-3-662-46761-9 ISBN 978-3-662-46762-6 (eBook)
DOI 10.1007/978-3-662-46762-6

Library of Congress Control Number: 2014950797

Springer Heidelberg New York Dordrecht London

Cover design: Jim Wilkie
Project copy editor: Christine Cressy
Author-generated LaTex, processed by EDV-Beratung Herweg, Germany

Printed on acid-free paper

Springer-Verlag GmbH Berlin Heidelberg is part of Springer Science+Business Media (www.springer.com)

Contents

List of Contributors

Baize, Rosemary R.
NASA Langley Research Center
Mail Stop 420
Hampton
VA 23681
USA
rosemary.r.baize@nasa.gov

Berdnik, Vladimir V.
Kazan Federal University
18 Kremlyovskaya Str.
Kazan
420008
Russia
berdnik@pochta.ru

Bi, Lei
Department of Atmospheric Sciences
Texas A&M University
College Station
TX 77843
USA
bilei@tamu.edu

Harmel, Tristan
Université Pierre et Marie Curie
Laboratoire Océanographie de Villefranche
06230 Villefranche sur Mer
France
harmel@obs-vlfr.fr

Hioki, Souichiro
Department of Atmospheric Sciences
Texas A&M University
College Station
TX 77843
USA
s.hioki@tamu.edu

Horvath, Helmuth
University of Vienna
Faulty of Physics
Aerosol and Environmental Physics
Boltzmanngasse 5
1090 Vienna
Austria
Helmuth.Horvath@univie.ac.at

Hu, Yongxiang
NASA Langley Research Center
Mail Stop 420
Hampton
VA 23681
USA
yongxiang.hu-1@nasa.gov

Huang, Xin
Department of Atmospheric Sciences
Texas A&M University
College Station
TX 77843
USA
huangxin.tamu@gmail.com

Kattawar, George W.
Department of Physics & Astronomy
Texas A&M University
College Station
TX 77843
USA
kattawar@physics.tamu.edu

Lin, Bing
NASA Langley Research Center
Mail Stop 420
Hampton
VA 23681
USA
bing.lin-1@nasa.gov

Loiko, Valery A.
B.I. Stepanov Institute of Physics of the
National Academy of Sciences of Belarus
Nezaleznasti Avenue 68
Minsk
Belarus
loiko@dragon.bas-net.by

Lukashin, Constantine
Mail Stop 420
NASA Langley Research Center
Hampton
VA 23681
USA
constantine.lukashin-1@nasa.gov

Panchenko, Mikhail Vasilievich
V.E. Zuev Institute of Atmospheric Optics
Tomsk
Russia
pmv@iao.ru

Savenkov, Sergey N.
Department of Radiophysics
Kyiv Taras Shevchenko University
Kyiv
Ukraine
sns@univ.kiev.ua

Sun, Wenbo
Mail Stop 420
NASA Langley Research Center
Hampton
VA 23681
USA
wenbo.sun-1@nasa.gov

Videen, Gorden
US Army Research Laboratory
2800 Powder Mill Road
Adelphi
MD 20783
USA
gorden.videen@us.army.mil

Xie, Yu
Department of Atmospheric Sciences
Texas A&M University
College Station
TX 77843
USA
xieyupku@gmail.com

Yang, Ping
Department of Atmospheric Sciences
Texas A&M University
College Station
TX 77843
USA
pyang@tamu.edu

You, Yu
Department of Physics & Astronomy
Texas A&M University
College Station
TX 77843
USA
youyu3@gmail.com

Zhuravleva, Tatyana B.
V.E. Zuev Institute of Atmospheric Optics
Tomsk
Russia
ztb@iao.ru

Preface

This volume of *Light Scattering Reviews* is aimed at the discussion of modern problems in polarized light radiative transfer, atmospheric optics, and remote sensing.

The first paper, prepared by Kattawar et al., is devoted to a thorough review of polarized light scattering in the atmosphere and ocean. Presented is a brief review of the history of the study of light-polarization properties. The utilization of light polarization can be traced to the use of sunstones by Vikings in sailing navigation. Many famous scientists, including Thomas Young, Etinne-Louis Malus, and Dominique Francois Arago, substantially contributed to enhancing the knowledge of light-polarization properties. The concepts and terminology introduced by pioneers remain in use today. In this chapter, the authors revisit the basic formalisms of the polarization characteristics of light within the framework of the Stokes parameters and Mueller matrix. In addition, the neutral points in the atmosphere and ocean and polarotaxis for marine animals are discussed. To illustrate the applications of the polarization of radiation, it is shown that the polarimetric observations made by a passive space-borne polarimeter, the POLDER-3 instrument aboard the PARASOL (Polarization and Anisotropy of Reflectances for Atmospheric Sciences, coupled with observations from a lidar) satellite platform can be used to effectively infer the microphysical properties of atmospheric ice crystals and dust particles, particularly the degree of surface roughness of ice crystals and the aspect ratios of dust particles.

Harmel discusses recent developments in the use of light polarization for the studies of marine environment from space. Radiometric measurements by satellite sensors of the light field backscattered from the atmosphere–ocean system represent a powerful tool to monitor marine ecosystems, carbon cycle, or water quality on the global scale. Estimations from space of the chlorophyll-a concentration and the subsequent estimate of the marine primary production, for instance, are currently being based on multispectral measurements of the water-leaving radiance regardless of its state of polarization. On the other hand, new investigations have been focused on the exploitation of polarization of light in the water column and exiting the sea surface to improve our capacities of observing and monitoring coastal and oceanic environments. This chapter attempts to give a brief overview of the recent developments on the use of polarization for marine environment monitoring including assessment of aerosol and atmospheric correction, sea state and associated winds, oceanic and coastal water content, and, potentially, estimation of the ocean carbon stock. First, a short historical review of the successive discoveries punctuated our understanding of light polarization in the marine environment is given. After a description of the transfer of light in the atmosphere–ocean system, impacts of the

water constituents (i.e., suspended particles, absorbing material) on polarization are summarized. Recent illustrations of the use and exploitation of light polarization for studying marine environment from laboratory to satellite applications are given. Through the chapter, benefits of polarimetric measurements for monitoring ocean, coastal, or lake environments are discussed in view of the future launch of polarimetric Earth-observing satellite missions.

Polarimetric investigations of terrestrial surfaces are discussed by Savenkov. To develop polarimetric methods for scattering scenes identification and classification, one needs to understand the relation between polarimetric and physical properties of the scatterers. Polarization properties of the scattered light contain extensive information on morphological and functional properties of the scatterers. Since polarization of scattered light depends on the morphological and physical parameters of scatterers (i.e., density, size, distribution, shape, refractive index, etc.) forming the studied object, this information can be utilized for making the scatterers identification techniques. Many constituents of a scattering object also exhibit polarization properties such as birefringence, dichroism, and depolarization which might serve to discriminate between surface and volume scattering as well. The importance of the optical and radar matrix polarimetry is that it contains all the information that one can obtain from the scattering scene. The polarimetric information has many useful applications in such diverse fields as interaction with various optical systems, cloud diagnostics, remote sensing of the ocean, atmosphere, and planetary surfaces, and biological tissue optics. The goal of the chapter is to explain the basics of polarimetry, outline its current state of the art, and review numerous important applications to characterize the terrestrial scattering both in optical range and in radar polarimetry.

Sun et al. present the results of polarized radiative-transfer modeling in the ocean–atmosphere-coupled system. Reflected solar radiation from Earth's ocean–atmosphere system is polarized. If a non-polarimetric radiometric sensor is sensitive to polarization, it will be a source of measurement errors in satellite remote sensing. To correct the errors due to this effect, the polarization state of the reflected solar light must be known with sufficient accuracy. In this chapter, recent studies of the polarized solar radiation for the ocean–atmosphere system with the adding-doubling radiative-transfer model are reviewed. The comparison of the modeled polarized solar radiation quantities with the PARASOL satellite measurements and other radiative-transfer model results, the sensitivities of reflected solar radiation's polarization to various ocean-surface and atmospheric conditions, and a novel super-thin cloud detection method based on polarization measurements are the focus of this chapter.

Panchenko and Zuravleva stress the importance of the aerosol vertical structure for radiative-transfer studies. In this chapter, the authors present a brief overview of the studies devoted to the problems of retrieving vertical profiles of microphysical and optical characteristics of tropospheric aerosols and their subsequent application in radiation calculations. The focus is on the descriptions of the approaches, which have been used to solve these tasks in the course of (i) specific comprehensive experiments and (ii) long-term observations (optical and microphysical approaches, method of microphysical extrapolation). Results obtained during the specific comprehensive experiments (TARFOX, ACE-2, SAFARI, SHADE) were performed by

different research groups with the use of instruments installed on board aircraft, ships, and satellites, as well as ground-based equipment. This ensured the implementation of aerosol and radiative closure tests to examine the magnitude of the uncertainties associated with the various techniques used to estimate the vertical structure of certain types of aerosols. Multi-year aircraft observations, which are held in a pre-determined area of the planet, are the basis for models of vertical profiles of climatically significant aerosol parameters specific for this region. The authors discuss the approaches which made it possible (i) to reveal the seasonal differences in the vertical profiles of the optical properties of dry matter aerosol in the visible range over the territory of rural Oklahoma (US) and (ii) to create the empirical model of the vertical profiles of the extinction coefficient, albedo, and scattering-phase function developed for the territory of Western Siberia (Russia).

Horwath discusses the aerosol absorption effects in the terrestrial atmosphere. Light absorption in the atmosphere is due to gases and particles. Most of them show considerable spatial and temporal variations. In the visible, broadband light absorption is due to O_3 and NO_2. Oxygen has some absorption lines. Ozone has a strong absorption in the ultraviolet (UV), shielding the short-wave UV radiation of the Sun. Also, SO_2 is absorbing in the near UV, allowing tracing of plumes. In the infrared (IR) water vapor, CO_2, CH_4, N_2O, halogenated hydrocarbons are strongly absorbing, leading to the well known greenhouse effect. Particles containing elemental (black) carbon, hematite, or other colored substances absorb, but also scatter, light. For particle sizes below 30 nm, the scattering is small compared to absorption. Coating absorbing particles or mixing with a transparent substance enhances the light absorption – that is, the mixed particle absorbs more light than the sum of the absorption of its constituents. The most important light-absorbing substance in atmospheric particles is black (graphitic) carbon, formed during combustion, and thus omnipresent. Since graphite is a conductor, the electrons can absorb any portion of energy, therefore absorbing in the visible, UV, and IR. A slight dependence of the absorption coefficient on wavelength mainly is an effect of the particle size. The nearly black mineral hematite (α-Fe_2O_3) is strongly absorbing up to wavelengths of approximately 600 nm due to a band gap of 1.9–2.2 eV. About 10% of the organic carbon in the atmosphere has a brown appearance and thus is called brown carbon. Humic-like substances (HULIS), particles formed in biomass fires, plant debris and degradation products, soil humics, and atmospheric reaction products can have this property. Again, the light absorption of these particles is higher in the short-wavelength range. The light absorption by pure gases (having negligible light scattering) can be measured by well-established standard technologies. When aerosol particles interact with light, in addition to absorption, the scattering of light by the particles is unavoidable. This complicates the absorption measurement.

Berdnik and Loiko discuss the application of neural networks for optical particle characterization. The review of neural networks to retrieve size and refractive index of homogeneous particles by angular dependence of the single light scattering is presented. Operating principles and training methods of the Multilayer Perceptron Neural Networks (MLP NN), Radial Basis Function Neural Networks (RBF NN), High-Order Neural Networks (HO NN), and Sequences of Neural Networks are discussed and evaluated for the problem considered. The basic part of the ar-

ticle relates to the homogeneous spherical particle characteristics retrieval. Some data on retrieval of characteristics of the absorbing particles and sizing of soft spheroidal particles are discussed as well. The problem on the retrieval of sizes of an individual optically soft particle taken from binary mixtures of either oblate and prolate spheroids or cylinders and oblate spheroids is considered. The multilevel neural networks method with a linear activation function and the method of the discrimination functions are used.

This volume of Light Scattering Reviews is dedicated to the memory of Georgii V. Rozenberg (1914–82), who made outstanding contributions in various branches of atmospheric optics, remote sensing, and radiative transfer.

Darmstadt, Germany *Alexander Kokhanovsky*
December 2014

Part I

Polarimetry

1 Polarization of light in the atmosphere and ocean

George W. Kattawar, Ping Yang, Yu You, Lei Bi, Yu Xie, Xin Huang, and Souichiro Hioki

1.1 Introduction

In this chapter, we will present a brief history of polarization, a short description of the Stokes parameter–Mueller matrix representation of polarized light, and techniques for using polarization for remote sensing of both the atmosphere and the ocean. For a collection of the diverse applications of polarization, the reader is referred to the excellent books by Gehrels (1974) and Mishchenko et al. (2010).

The use of polarization for navigation, sustenance, and recognition by both terrestrial and marine organisms has been in effect for several hundred million years. The *raison d'être* is that both skylight and underwater light can be strongly polarized, and nature has found a way for many organisms to utilize this property. Extensive research on skylight polarization has been undertaken as atmospheric observations are quite a natural part of our daily routine, and blue skylight is a source of polarized light. Perhaps because man is not a resident of the sea, research on the polarization properties of the ocean and the hydrosols contained therein has, unfortunately, been very limited.

1.2 Brief history of polarization

A more complete history of polarization can be found in the references (Brosseau, 1998) and at *www.polarization.com/*.

Whether the Vikings found their way to America by using skylight polarization as a navigational compass (Roslund and Beckman, 1994; Dougherty, 2013) by looking at the sky through a crystal, oftentimes referred to as a sunstone, is certainly speculative. The Vikings' amazing sailing achievements were made before the magnetic compass reached Europe from China, and the mechanics of steering a true course on their long voyages out of land sight, especially in the frequent bad weather and low visibility at high latitudes, are still in question. Six and a half centuries elapsed before other polarization properties were reported. Before the end of the 17th century, Erasmus Bartholinus had discovered the birefringence (double refraction) of calcite, $CaCO_3$, from the observation of double images viewed

A.A. Kokhanovsky, *Light Scattering Reviews 10*, Springer Praxis Books,
DOI 10.1007/978-3-662-46762-6_1

through the crystals, and wrote a 60-page memoir discussing his results (Bartholinus, 1670). He was the first to use the terms 'ordinary ray' and 'extraordinary ray,' which remain in use today. Roughly three years later, Christiaan Huygens explained the double-refraction property of calcite by extending the geometric construction method he used to explain refraction. Huygens (using what we now call the Huygens Principle) realized that, if the speed of light varied with direction, the spherical wavefronts would metamorphose into ellipsoids which would explain the double-refraction property of the crystals. Following the turn of the nineteenth century, rapid discoveries of the polarization properties of various materials and natural media were made. In 1801, the brilliant Thomas Young, who many historians believe deciphered the Egyptian Hieroglyphs before Champollion, illustrated that polarization arose from the transverse nature of light. In 1808, Etienne-Louis Malus, after surviving the French revolution, discovered that polarized light was not restricted only to certain crystals but could be generated by the reflection of sunlight from ordinary surfaces (Malus, 1808). From his experiments, Malus was able to deduce what we now call Malus's Law relating the quantity of transmitted light to the relative position of a polarizing filter when viewing polarized light. These first findings seemed to create a great deal of research activity dealing with polarization. In 1812, Sir David Brewster (probably best known for his discovery of the kaleidoscope), an ex-minister in the church of Scotland, repeated many of Malus's experiments and was able to conclude: 'The index of refraction is the tangent of the angle of polarization' and 'when a ray is polarized by reflection, the reflected ray forms a right angle with the refracted ray.' As history has it, the angle is called the 'Brewster angle' with no credit being given to Malus – an example of Stigler's Law of Eponymy, which states that 'No scientific discovery is named after its original discoverer.' Around 1811, Dominique Francois Arago, while observing interference colors by placing a thin sheet of mica between a glass reflector and a calcite prism, noticed the colors did not disappear when he removed the reflector leaving only blue sky as the background. From this observation, he immediately deduced that blue sky must indeed be polarized! Arago also saw circular polarization when the mica was replaced by a quartz crystal, which we know to be birefringent, and presented his findings to the Paris Academy. Unfortunately, a year later, a former colleague named Jean-Baptiste Biot presented two much more detailed papers and stole the limelight from Arago, and now Biot is sometimes credited with the discovery of circular polarization. One of Arago's greatest accomplishments was his persistence in convincing the brilliant mathematical physicist Augustin Fresnel to keep pursuing optics. Fresnel once stated, 'I have decided to remain a modest engineer ... and even abandon physics ... I now see it as a stupid plan troubling oneself to acquire a small bit of glory.' In 1816, Fresnel developed his theory of diffraction without mentioning polarization but, later that year and in the next year, Fresnel theoretically explained the existence of polarization as well as reflection, refraction, and Brewster's Law. Around 1821, Fresnel discovered that, if light waves were indeed transverse, he could explain many earlier experiments, and went on to show that two light beams polarized at right angles to one another do not interfere (note that many researchers are not familiar with Fresnel and Arago's four laws of interference, which are not usually covered in most modern optics books, and the reader is referred to an article by Collett (1971)). More optical phenom-

ena, such as polarized rotation of quartz and various fluids, linear polarization of reflected light, polarization of comet tails, neutral points (points with no polarization) in the sky, rainbows, and 22° halos, were either discovered or explained in rapid sequence. For the next century and a half, improvements were made in the construction of efficient linear polarizers, and more observations of the polarization effects of natural phenomena were reported. Furthermore, the Lorenz–Mie theory for the scattering of light by small spheres (Lorenz, 1890; Mie, 1908; van de Hulst, 1981) has been a powerful tool to facilitate the theoretical explanation of the polarization characteristics associated with atmospheric scattering phenomena, such as rainbows, blue sky polarization, and glory (a bright, halo-like optical pattern due to the backscattering of light by a cloud of uniformly sized water droplets). Note, a quite extensive review of the history of the Lorenz–Mie theory can be found in Logan (1965).

1.3 Stokes–Mueller formulation

William B. Herapath, an English physician and surgeon, discovered linear dichroism in crystals in what is now known as herapathite. After this, Sir George Stokes introduced the four measurable quantities completely describing the state of polarization of a light beam, which we now call the Stokes parameter or Stokes vector (note that vector is not used in the mathematical sense). Once Edwin Land was able to make the first sheet polarizers by orienting crystalline needles of herapathite in a sheet of plastic, the use of polarization techniques began to blossom. People began to focus on how the state of polarization of a light beam changed when it interacted with optical elements such as polarizers, quarter-wave plates, etc. Soleillet (1929) was one of the first pioneers to suggest how one might characterize an optical device by relating the output Stokes vector to the input Stokes vector; however, his elegant paper received virtually no attention. Soleillet's method was rediscovered by Hans Mueller, who used these matrices in a series of lectures given at MIT from 1945 to 1948, and now the 4×4 matrix transformations bear the name *Mueller matrices* – another example of Stigler's Law of Eponymy at work. Mueller did not publish the work in the open literature, but the theory was later published by N.G. Parke, an MIT student, as part of his Ph.D. dissertation. Another polarization pioneer was Robert C. Jones, who was interested in the optical properties of birefringence and dichroism, and developed a method of transformations which used 2×2 matrices. The method had several limitations, of which one of the most important was being only specific to polarized light beams.

The polarized nature of the underwater light field was discovered over half a century ago, and has been found to aid in target identification and to be detected and utilized by a variety of marine animals. Waterman (1954) and Waterman and Westell (1956) probably made the earliest measurements of the polarized underwater light field and studied the sensitivity of the polarization state to the solar and viewing configuration. Substantially polarized light fields (75% to 80%) in the clear waters near Bermuda were observed by Ivanoff et al. (1961). The laboratory measurements made by Timofeeva (1974) showed a value of the degree of linear polarization (DoLP) as high as 40% in turbid waters. The more recent work

on ocean-water polarization includes the large RaDyO (Radiation in a Dynamic Ocean) project (Dickey et al., 2011). The work of Sabbah and Shashar (2007) is the most comprehensive combination of both measurement and theory brought to the fore. As shown by Chami (2007), underwater polarization can also be used by remote sensing to study the optical signature of inorganic particles in coastal waters.

Multispectral underwater polarization properties have drawn a great deal of attention in the experimental biology community, particularly in the study of the impact of light polarization state on marine animals. Evidence has shown that some marine animals are able to detect both the DoLP and the angle of linear polarization (AoLP) specified by the orientation of the electric field vector; therefore, both are important. The impact of atmospheric conditions and water compositions on underwater polarized light fields was discussed by Tonizzo et al. (2009), who reported a hyperspectral and multangular analysis of polarized light in coastal waters.

An alternative approach to study underwater polarization is model simulation, which has been conducted since numerical models that solve the vector radiative-transfer equation became available in the 1970s. Such models include the Multi-Component Approximation (MCA) (Tynes et al., 2001) and the Monte Carlo (Kattawar et al., 1973) methods. With appropriate input parameters including solar irradiance, atmospheric conditions, aerosol loading, and water inherent optical properties (IOPs) in numerical simulations, close agreement has been achieved between theoretical and measured radiances and polarization states. In particular, comparisons between simulated and measured underwater polarized light fields (Adams et al., 2002; Tonizzo et al., 2009; You et al., 2011) demonstrate reasonable consistency in the cases of both the DoLP and the AoLP.

1.4 Stokes parameters

Polarization parameters of light are generally referred to specific planes. Precision is required when defining the planes to which the Stokes vector is referred when considering the polarization of light in radiative-transfer calculations. For a scattered beam in a single-scattering process, a natural selection is the scattering plane defined by the propagation directions of the incident beam and the scattered beam. The radiance of beams can be resolved into two orthogonal components referring to the vibrations of the electric field parallel and perpendicular to the scattering plane. In radiative-transfer calculations, the polarization parameters of a pencil of light are usually defined with respect to meridional planes. If we consider Fig. 1.1, and denote the radiance associated with the incident beam by I_{inc} and the counterpart of the scattered beam by I_{sca}, the directions of the incident beam and the scattered beam determine the scattering plane (the scattering angle is denoted as Θ), and the directions of two beams and the z-axis define two meridional planes. In addition to the reference plane, a proper treatment of the Stokes vector formulation requires careful consideration of relevant definitions due to various freedoms of choice.

Let us consider the meridional plane defined by the directions of the incident beam and the z-axis. Two orthogonal unit vectors $\hat{e}_1$ and $\hat{e}_2$ in the meridional plane

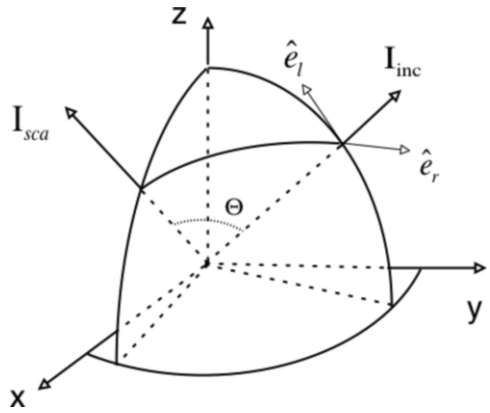

Fig. 1.1. Reference planes used for describing the Stokes vector.

and perpendicular to the plane are defined in such a way that $\hat{e}_r \times \hat{e}_l$ is aligned with the direction of propagation (note this is one of the freedoms of choice; switching $\hat{e}_l$ and $\hat{e}_r$ will result in differences in the foregoing definitions; most texts in the literature adopted this convention but, in Mishchenko et al. (2000), $\hat{e}_\varphi$ and $\hat{e}_\theta$ are used to represent the directions perpendicular and parallel to the meridional plane). Based on the transverse nature of local electromagnetic waves, the electric field vector in conjunction with the incident beam can be resolved into two components:

$$\overline{E} = E_l \hat{e}_l + E_r \hat{e}_r \,, \tag{1.1}$$

where E_l and E_r are complex oscillatory functions with respect to the propagation distance and time. The Stokes vector with four real components can be defined as

$$\begin{bmatrix} I \\ Q \\ U \\ V \end{bmatrix} = \begin{bmatrix} |E_l|^2 + |E_r|^2 \\ |E_l|^2 - |E_r|^2 \\ E_l E_r^* + E_r E_l^* \\ i(E_l E_r^* - E_r E_l^*) \end{bmatrix} , \tag{1.2}$$

where $|\cdot|$ denotes the modulus, the asterisk denotes complex conjugation, and $i = (-1)^{1/2}$. It can be proven that the following relation holds:

$$I^2 = Q^2 + U^2 + V^2 \,. \tag{1.3}$$

The first component I is commonly referred to as the radiance (in most texts, I represents irradiance in single scattering) and the other three parameters have the same units as I. The definition of Eq. (1.2) is consistent with the literature (van de Hulst, 1981; Bohren and Huffman, 1983). Liou (2002) included a minus sign into the definition of the V component. The freedom of sign choice in the definition of the V component is also mixed with the convention adopted in representing the time dependence of harmonic waves. The wave is propagating along the z-axis, in van de Hulst (1981) and Liou (2002) it is

$$E_l = a_l \, e^{-i\varepsilon_l} \, e^{-ikz+i\omega t}, \quad E_r = a_r \, e^{-i\varepsilon_r} \, e^{-ikz+i\omega t} \,, \tag{1.4}$$

while, in Bohren and Huffman (1983), it takes the form

$$E_l = a_l\, e^{-i\varepsilon_l}\, e^{ikz-i\omega t}, \quad E_r = a_r\, e^{-i\varepsilon_r}\, e^{ikz-i\omega t}\,, \tag{1.5}$$

where t is the time, a_l and a_r are real numbers that represent amplitudes, ε_1 and ε_2 are the phases of the wave at the spatial origin of space at time $t = 0$, k is the modified wave number, and ω is the circular frequency. Both Eqs (1.4) and (1.5) lead to

$$\begin{bmatrix} I \\ Q \\ U \\ V \end{bmatrix} = \begin{bmatrix} a_l^2 + a_r^2 \\ a_l^2 - a_r^2 \\ 2a_r a_l \cos\delta \\ 2a_r a_l \sin\delta \end{bmatrix}, \tag{1.6}$$

and $\delta = \varepsilon_l - \varepsilon_r$. However, if the simple waves

$$E_l = a_l\, e^{i\varepsilon_l}\, e^{ikz-\omega t}, \quad E_r = a_r\, e^{i\varepsilon_r}\, e^{ikz-i\omega t}\,, \tag{1.7}$$

are employed, the V component will have an opposite sign. Note that the adoption of a different time factor will lead to a complex refractive index with an opposite sign for the imaginary part, and the sign difference of the V component will result in sign differences of the first three Mueller matrix elements in the fourth row or column. Moreover, the sign difference of the V component will cause confusion in the definition of left-handed and right-handed circular light. Note that the I, Q, and U components in Eq. (1.6) are immaterial to the choice of the time dependence, but the sign of the V component depends on both the sign choice in Eq. (1.2) and the representation of harmonic waves in Eq. (1.5).

Consider the most general state of polarization, namely elliptical polarization, where the axes of the ellipse may not be in the $\hat{e}_l$ and $\hat{e}_r$ directions. Let $\hat{p}$ and $\hat{q}$ be orthogonal unit vectors that align with the semi-major and semi-minor axes of the polarization ellipse (see Fig. 1.2). A geometric description of the simple wave can be written as

$$\mathrm{Re}\,(\vec{E}) = \hat{p}a_p \cos(kz - \omega t + \alpha) + \hat{q}a_q \sin(kz - \omega t + \alpha)\,. \tag{1.8}$$

Note that the two components along the $\hat{p}$ and $\hat{q}$ directions satisfy the ellipse equation with the semi-axis of $|a_p|$ and $|a_q|$, and α is an arbitrary phase angle. Because the radiance should be independent of the choice of the representation, the following equation must be satisfied:

$$a_p^2 + a_q^2 = a_l^2 + a_r^2\,. \tag{1.9}$$

For convenience, an auxiliary angle $\beta \in [0, \pi/2]$ is introduced, such that

$$a_p = a\cos\beta, \quad a_q = a\sin\beta, \quad a = \sqrt{a_r^2 + a_l^2}\,. \tag{1.10}$$

With the projection of the electric field given by Eq. (1.8) to the $\hat{e}_l$ and $\hat{e}_r$ directions, we have

$$\begin{aligned} &a\cos\beta\cos(kz - \omega t + \alpha)\cos\chi - a\sin\beta\sin(kz - \omega t + \alpha)\sin\chi \\ &\quad = a_l\cos(kz - \omega t + \varepsilon_1)\,, \end{aligned} \tag{1.11}$$

$$\begin{aligned} &a\cos\beta\cos(kz - \omega t + \alpha)\sin\chi + a\sin\beta\sin(kz - \omega t + \alpha)\cos\chi \\ &\quad = a_r\cos(kz - \omega t + \varepsilon_2)\,. \end{aligned} \tag{1.12}$$

In Eqs (1.11) and (1.12), χ is the angle between $\hat{p}$ and $\hat{e}_l$. Because of the arbitrary position and time, the coefficients of $\cos(kz - \omega t)$ and $\sin(kz - \omega t)$ on both sides of Eqs (1.11) and (1.12) must be the same. Then, we have

$$a\cos\beta\cos\alpha\cos\chi - a\sin\beta\sin\alpha\sin\chi = a_l\cos\varepsilon_1\,, \tag{1.13}$$

$$a\cos\beta\sin\alpha\cos\chi + a\sin\beta\cos\alpha\sin\chi = a_l\sin\varepsilon_1\,, \tag{1.14}$$

$$a\cos\beta\cos\alpha\sin\chi + a\sin\beta\sin\alpha\cos\chi = a_r\cos\varepsilon_2\,, \tag{1.15}$$

$$-a\cos\beta\sin\alpha\sin\chi + a\sin\beta\cos\alpha\cos\chi = -a_r\sin\varepsilon_2\,. \tag{1.16}$$

Based on Eqs (1.13)–(1.16), the Stokes vector can be written with respect to the amplitude and the orientation angle as depicted in Fig. 1.2. On squaring and adding Eqs (1.13) and (1.14), we obtain the intensity along the $\hat{e}_l$ direction

$$a_l^2 = a^2\left(\cos^2\beta\cos^2\chi + \sin^2\beta\sin^2\chi\right)\,. \tag{1.17}$$

Similarly, from Eqs (1.15) and (1.16), we have

$$a_r^2 = a^2\left(\cos^2\beta\sin^2\chi + \sin^2\beta\cos^2\chi\right)\,. \tag{1.18}$$

Adding the product of Eq. (1.13) and (1.15), and that of (1.14) and (1.16) yields

$$2a_r a_l\cos\delta = a^2\cos 2\beta\sin 2\chi\,, \tag{1.19}$$

where $\delta = \varepsilon_1 - \varepsilon_2$. Adding the product of Eq. (1.14) and (1.15), and that of (1.13) and (1.16) yields

$$2a_r a_l\sin\delta = a^2\sin 2\beta\,. \tag{1.20}$$

Based on Eqs (1.13) and (1.14), we have

$$\frac{\text{Eq.[13]}\times\cos\alpha + \text{Eq.[14]}\times\sin\alpha}{\text{Eq.[13]}\times\sin\alpha - \text{Eq.[14]}\times\cos\alpha} \Rightarrow \tan(\alpha - \varepsilon_1) = -\tan\beta\tan\chi\,. \tag{1.21}$$

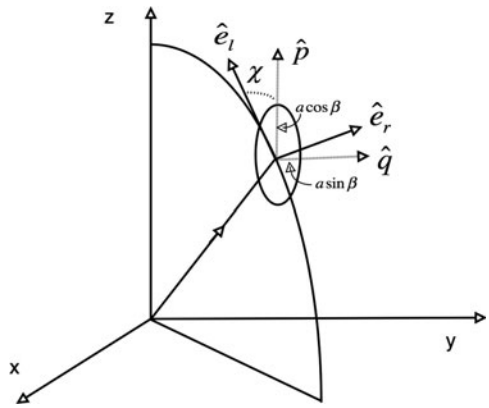

Fig. 1.2. Geometric description of an elliptical wave using the representation.

Similarly, we have

$$\frac{\text{Eq.}[15] \times \cos\alpha - \text{Eq.}[16] \times \sin\alpha}{\text{Eq.}[15] \times \sin\alpha + \text{Eq.}[16] \times \cos\alpha} \Rightarrow \tan(\alpha - \varepsilon_2) = \tan\beta \cot\chi\,, \tag{1.22}$$

therefore

$$\tan\delta = \tan\left[(\alpha - \varepsilon_2) - (\alpha - \varepsilon_1)\right] = -\frac{\tan 2\beta}{\sin 2\chi}\,. \tag{1.23}$$

Note that the sine and cosine terms can be formally switched to represent the geometry of the polarization. In that case, Eqs (1.17), (1.18), (1.19), (1.20), and (1.23) will not be changed, but Eqs (1.21) and (1.22) will be given by

$$\tan(\alpha + \varepsilon_1) = -\cot\beta \cot\chi\,, \tag{1.24}$$

$$\tan(\alpha + \varepsilon_2) = \cot\beta \tan\chi\,. \tag{1.25}$$

Based on Eqs (1.6), (1.17), (1.18), (1.19), and (1.20), the Stokes parameters in the geometric notation now become (van de Hulst, 1981)

$$\begin{bmatrix} I \\ Q \\ U \\ V \end{bmatrix} = \begin{bmatrix} a^2 \\ a^2 \cos 2\beta \cos 2\chi \\ a^2 \cos 2\beta \sin 2\chi \\ a^2 \sin 2\beta \end{bmatrix}\,. \tag{1.26}$$

Note that Q, U, and V are spherical coordinates, which can be represented in a Poincare sphere (Born and Wolf, 2001).

Given the Stokes vector, it is straightforward from Eq. (1.26) to obtain the orientation of the polarization ellipse, $\tan 2\chi = U/Q$ and the ellipticity $\tan 2\beta = V/(Q^2 + U^2)^{1/2}$. Other quantities extracted from the Stokes vector which are used quite often when discussing polarization states, namely the degree of polarization, $(Q^2 + U^2 + V^2)^{1/2}/I$, the DoLP, $(Q^2 + U^2)^{1/2}/I$, and the degree of circular polarization, $|V|/I$.

The Stokes parameters can be defined with respect to different planes of reference, such as the scattering plane or the meridional plane as seen Fig. 1.1. For convenience, in Fig. 1.3, we consider two reference planes with an intersection angle of ϕ. The relationship between the two sets of Stokes parameters is easily shown to be

$$\begin{bmatrix} I' \\ Q' \\ U' \\ V' \end{bmatrix} = \mathbf{R}(\phi) \begin{bmatrix} I \\ Q \\ U \\ V \end{bmatrix} = \begin{bmatrix} 1 & 0 & 0 & 0 \\ 0 & \cos 2\phi & \sin 2\phi & 0 \\ 0 & -\sin 2\phi & \cos 2\phi & 0 \\ 0 & 0 & 0 & 1 \end{bmatrix} \begin{bmatrix} I \\ Q \\ U \\ V \end{bmatrix}\,, \tag{1.27}$$

where ϕ is defined as the clockwise rotation angle of the $\hat{e}_l$-axis to the $\hat{e}'_l$-axis, and the reader is facing the propagation direction of the beam. The rotation matrix warrants I, $Q^2 + U^2$ and V to be invariant. As expected, the degree of polarization, the DoLP, the degree of circular polarization, and the ellipticity are independent of the plane of reference. The rotation matrix $\mathbf{R}(\phi)$ defined in Eq. (1.27) has some other important properties, namely:

$$\begin{aligned} \mathbf{R}(-\phi) &= \mathbf{R}(\pi - \phi) \\ \mathbf{R}(\phi_1)\mathbf{R}(\phi_2) &= \mathbf{R}(\phi_1 + \phi_2) \\ \mathbf{R}^{-1}(\phi) &= \mathbf{R}(-\phi) \end{aligned} \tag{1.28}$$

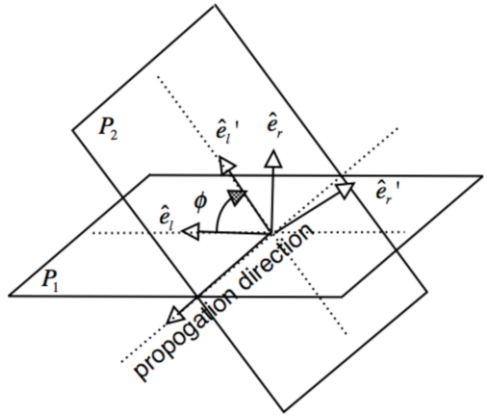

Fig. 1.3. A clockwise rotation by an angle ϕ of the two axes for the Stokes vector representation.

To measure the Stokes parameters associated with a light beam, the measurement set-up schematically illustrated in Fig. 1.4 can be used. The compensator, also called a wave plate or retarder, introduces a certain amount of retardation in the phase of one of the two components of the electric field decomposed with respect to the $\hat{e}_l$ and $\hat{e}_r$ directions. In the following discussion, we assume the phase difference between the $\hat{e}_l$ and $\hat{e}_r$ components of the electric field vector to be ε. The polarizer constrains the measurement of the electric field vector component to vibrating in only one direction and deviating from the $\hat{e}_r$-axis by an angle φ, which is called the direction of the transmission axis of the linear polarizer.

After algebraic manipulation (the details of which can be found in Chandrasekhar (1950)), the measured radiance is a function of ε and φ in the form of

$$I(\varepsilon, \varphi) = I_{i,l} \cos^2 \varphi + I_{i,r} \sin^2 \varphi + \frac{1}{2}(U_i \cos \varepsilon - V_i \sin \varepsilon) \sin 2\varphi \,, \tag{1.29}$$

where the subscript 'i' indicates the Stokes parameters associated with the incident beam. With Eq. (1.29), we consider the following four scenarios:

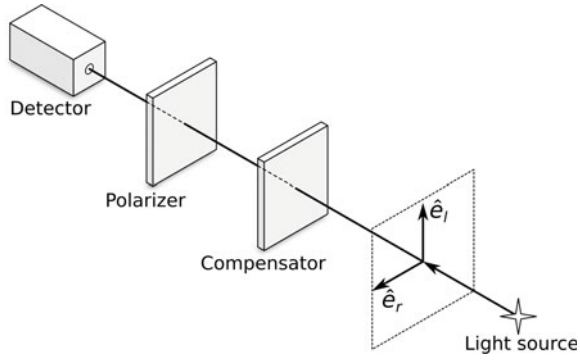

Fig. 1.4. Schematic diagram for measuring the Stokes parameters.

1. **No polarization** (i.e., the incident light is natural light), $I_{i,l} = I_{i,r} = I_i/2$, $U_i = 0$, and $V_i = 0$. Thus, we obtain

$$I(\varepsilon, \varphi) = I_{i,l} \cos^2 \varphi + I_{i,r} \sin^2 \varphi = \frac{I_i}{2}(\cos^2 \varphi + \sin^2 \varphi) = I_i/2 \tag{1.30}$$

or

$$I_i = 2I(\varepsilon, \varphi)\,. \tag{1.31}$$

2. **Horizontal and vertical polarization configurations without a compensator** (i.e., $\varepsilon = 0$, $\varphi = 0°$, and $\varphi = 90°$) for a polarized incident beam:

$$I(\varphi = 0°,\ \varepsilon = 0) = I_{i,l}\,, \tag{1.32}$$
$$I(\varphi = 90°,\ \varepsilon = 0) = I_{i,r}\,. \tag{1.33}$$

Using the above two equations, we obtain the first two Stokes parameters in the form of

$$I_i = I_{i,l} + I_{i,r} = I(\varphi = 0°,\ \varepsilon = 0) + I(\varphi = 90°,\ \varepsilon = 0)\,, \tag{1.34}$$
$$Q_i = I_{i,l} - I_{i,r} = I(\varphi = 0°,\ \varepsilon = 0) - I(\varphi = 90°,\ \varepsilon = 0)\,. \tag{1.35}$$

3. **+45° and −45° polarization configurations without a compensator** (i.e., $\varepsilon = 0$, $\varphi = 45°$, and $\varphi = -45°$) for a polarized incident beam:

$$I(\varphi = 45°,\ \varepsilon = 0) = \frac{1}{2}(I_{i,l} + I_{i,r}) + \frac{1}{2}U_i\,, \tag{1.36}$$
$$I(\varphi = -45°,\ \varepsilon = 0) = \frac{1}{2}(I_{i,l} + I_{i,r}) - \frac{1}{2}U_i\,. \tag{1.37}$$

Thus, we obtain

$$U_i = I(\varphi = 45°,\ \varepsilon = 0) - I(\varphi = -45°,\ \varepsilon = 0)\,. \tag{1.38}$$

4. **Measurement of circular polarization using +45° and −45° polarization configurations with a quarter-wave plate** ($\varepsilon = \pi/2$, $\varphi = 45°$, and $\varphi = -45°$)

$$I(\varphi = 45°,\ \varepsilon = \pi/2) = \frac{1}{2}(I_{i,l} + I_{i,r}) - \frac{1}{2}V_i\,, \tag{1.39}$$
$$I(\varphi = -45°,\ \varepsilon = \pi/2) = \frac{1}{2}(I_{i,l} + I_{i,r}) + \frac{1}{2}V_i\,, \tag{1.40}$$

Thus, we obtain

$$V_i = I(\varphi = -45°,\ \varepsilon = \pi/2) - I(\varphi = 45°,\ \varepsilon = \pi/2)\,. \tag{1.41}$$

Note that the foregoing measurements in scenarios (2)–(4) provide the Stokes parameters regardless of the polarization state of the incident beam. It should be pointed out that a thorough review of the polarized light, particularly light scattered by isotropic opalescent media, can be found in Perrin (1942).

1.5 Mueller matrices

We have shown a method to calculate the complete Stokes vector, and our next task is to determine the nature of the 4×4 matrix which transforms an incident Stokes vector into another Stokes vector due to the interaction between light and any object. The resulting matrix is called the Mueller matrix (Mueller, 1948) but, as pointed out earlier, was first discovered by Soleillet (1929). The matrix gives essentially all the optical information possible about an elastic scattering system where some interaction has occurred, and thus characterizes the optical properties of the involved scattering system. Many excellent references on the theory of Mueller matrices exist, but we refer the reader to the book by Shurcliff (1962).

As an example, we consider an ideal linear polarizer – that is, the compensator in Fig. 1.4 is removed (i.e., $\varepsilon = 0$) and Eq. (1.29) reduces to

$$I(\varphi) = I_{i,l} \cos^2 \varphi + I_{i,r} \sin^2 \varphi + \frac{1}{2} U_i \sin 2\varphi \,. \tag{1.42}$$

Using the relation $I_{i,l} \cos^2 \varphi + I_{i,r} \sin^2 \varphi = (I_i + Q_i \cos 2\varphi)/2$, the preceding equation can be further simplified in the form

$$I(\varphi) = \frac{1}{2}(I_i + Q_i \cos 2\varphi + U_i \sin 2\varphi) \,, \tag{1.43}$$

which is the first row of the following Mueller matrix associated with a linear polarizer (Bohren and Huffman, 1983), given by

$$\begin{bmatrix} I \\ Q \\ U \\ V \end{bmatrix} = \frac{1}{2} \begin{bmatrix} 1 & \cos 2\varphi & \sin 2\varphi & 0 \\ \cos 2\varphi & \cos^2 2\varphi & \cos 2\varphi \sin 2\varphi & 0 \\ \sin 2\varphi & \cos 2\varphi \sin 2\varphi & \sin^2 2\varphi & 0 \\ 0 & 0 & 0 & 0 \end{bmatrix} \begin{bmatrix} I_i \\ Q_i \\ U_i \\ V_i \end{bmatrix} . \tag{1.44}$$

Obviously, the linear polarizer is not able to generate the V component. Similarly, the Mueller matrix can characterize the optical properties of any optical element.

The Mueller matrices of the optical elements can be obtained in a straightforward manner because their optical properties are already known. For air–ocean interfaces, molecules, and particles involved in the atmospheric and oceanic radiative-transfer simulations, the Mueller matrices must be obtained from either physical principles or Maxwell's equations. Consider the dielectric surface between the atmosphere and the ocean; the Mueller matrices associated with the reflection and the transmission of light either from air to medium or medium to air have to be obtained from physical principles. For example, in the case of the air-to-medium reflection based on the Fresnel's reflection, the reflection Mueller matrix from air into a medium can be obtained as

$$R_{AM} = \begin{bmatrix} \alpha + \eta & \alpha - \eta & 0 & 0 \\ \alpha - \eta & \alpha + \eta & 0 & 0 \\ 0 & 0 & \gamma_{\mathrm{Re}} & 0 \\ 0 & 0 & 0 & \gamma_{\mathrm{Re}} \end{bmatrix} , \tag{1.45}$$

where

$$\alpha = \frac{1}{2}\frac{\tan^2(\theta_i - \theta_t)}{\tan^2(\theta_i + \theta_t)}, \tag{1.46}$$

$$\eta = \frac{1}{2}\frac{\sin^2(\theta_i - \theta_t)}{\sin^2(\theta_i + \theta_t)}, \tag{1.47}$$

$$\gamma_{\mathrm{Re}} = \frac{\tan(\theta_i - \theta_t)\sin(\theta_i - \theta_t)}{\tan(\theta_i + \theta_t)\sin(\theta_i + \theta_t)}. \tag{1.48}$$

In Eqs (1.46) and (1.47), α and η are reflectivities associated with polarization in the parallel and perpendicular directions. The Mueller matrices associated with the transmissivity and the scenarios from the medium to air can be similarly obtained (Kattawar and Adams, 1989).

To obtain the Mueller matrices for various particles, one must turn to Maxwell's equations. Based on the far-field approximation, the amplitude-scattering matrix is usually defined to transform the incident field to the scattered field:

$$\begin{bmatrix} E_\parallel \\ E_\perp \end{bmatrix} = \frac{e^{ikr}}{-ikr}\begin{bmatrix} S_2 & S_3 \\ S_4 & S_1 \end{bmatrix}\begin{bmatrix} E_{\parallel,i} \\ E_{\perp,i} \end{bmatrix}. \tag{1.49}$$

The scattered field by molecules, for particles much smaller than the incident wavelength, specifically, when $x \ll 1$ (Shifrin, 1951), can be easily obtained from Maxwell's equations, in which case the amplitude-scattering matrix is given by

$$\begin{bmatrix} S_2 & S_3 \\ S_4 & S_1 \end{bmatrix} \propto \begin{bmatrix} \cos\Theta & 0 \\ 0 & 1 \end{bmatrix}. \tag{1.50}$$

The Mueller matrix for Rayleigh scattering is given by

$$\frac{1}{2}\begin{bmatrix} \mu^2+1 & \mu^2-1 & 0 & 0 \\ \mu^2-1 & \mu^2+1 & 0 & 0 \\ 0 & 0 & \mu & 0 \\ 0 & 0 & 0 & \mu \end{bmatrix}, \tag{1.51}$$

where $\mu = \cos\Theta$ and Θ is the scattering angle. Several interesting features of the preceding matrix can be noted. In particular, complete linear polarization is noted at a scattering angle of 90°; ellipticity does not exist in the multiple-scattering-induced radiation if the source is unpolarized; and the relevant depolarization factor is zero.

The Mueller matrix for homogeneous spheres can be readily obtained from the Lorenz–Mie theory. However, the calculation is not trivial in mathematical and computational physics for arbitrarily shaped nonspherical particles. A number of numerical methods have been developed to obtain the Mueller matrix for particles within a limited size parameter range $(0, X_m)$ including the finite-difference-time-domain method (Yee, 1966; Yang and Liou, 1996a), the discrete-dipole-approximation method (Purcell and Pennypacker, 1973; Draine and Flatau, 1994; Yurkin et al., 2007), the separation of variables method (Asano,1979; Farafonov, 1983), and the T-matrix method (Waterman, 1971; Mishchenko and Travis, 1998; Mackowski and Mishchenko, 1996; Doicu et al., 2006; Kahnert, 2013; Bi et

al., 2013, and references therein). X_m depends on the particle shape, the refractive index, the computational resources, and the selected computational method. For large-sized parameters beyond the capabilities of numerical methods, a common approach is based on geometric-and-physical optics approximations. A review of the physical-geometric optics approximations for a solution of the optical properties of ice crystals and aerosols can be found in Bi and Yang (2013).

Before one can theoretically calculate the polarization of the submarine radiance fields (see Kattawar et al., 1973, 1988; Kattawar and Adams, 1989), the Mueller matrix for ocean water must be obtained. Beardsley (1968) performed the first measurement of the Mueller matrix for ocean-water samples. He noticed a great deal of symmetry in the matrices measured from different sources, and the normalized matrix element values were similar to those for a normalized matrix derived for Rayleigh scattering (presented earlier). Later measurements made by Soviet scientists (Kadyshevich, 1977; Kadyshevich et al., 1971, 1976) suggested much larger variations in the Mueller matrix as a function of depth and location. The apparent discrepancy was resolved by Voss and Fry (1984), who made Mueller matrix measurements in the Atlantic, Pacific, and Gulf of Mexico, and showed that the Mueller matrix has little variation between sites and confirmed Beardsley's Rayleigh-like appearance of the matrices. Shown in Fig. 1.5 is a depiction of P_{12}/P_{11}, P_{22}/P_{11}, and P_{33}/P_{11} for scattering angles from 10° to 160°. Note that P_{12}/P_{11} and P_{33}/P_{11} for the ocean-water average values are close to those for a Rayleigh-scattering simulation. Kokhanovsky (2003) presented the parameterization of the Mueller matrix of oceanic water measured by Voss and Fry (1984), which could be used for theoretical polarized radiative-transfer studies involving oceanic waters. One of the most important hydrosol observations was that the particles could not be spherical. The explanation is the normalized Mueller matrix element S_{22} was not unity and, for any spherical polydispersion, S_{22} must be unity. The zero values in the upper and lower 2 × 2 submatrices indicate little, if any, optical activity in the samples or preferred orientation by the particulates; however, this is not to suggest that highly

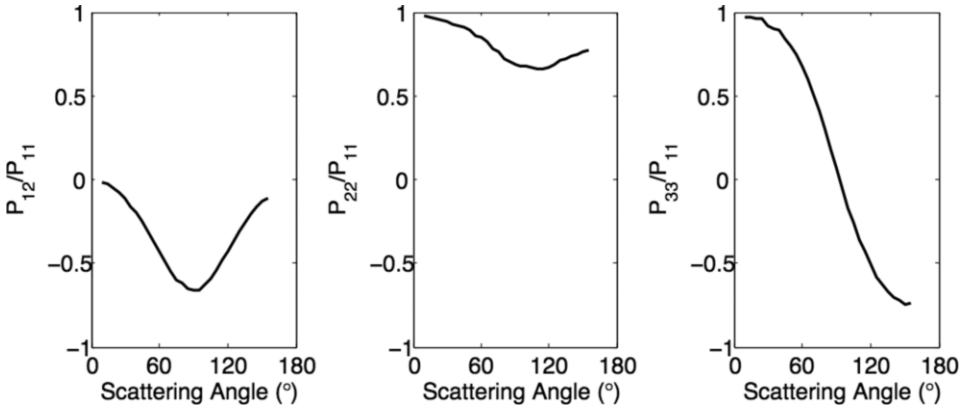

Fig. 1.5. Sample Mueller matrix elements (averaged values) regenerated from Voss and Fry (1984, Table VI). P_{21} is equal to P_{12}, and P_{44} is equal to P_{33}. All other elements associated with polarization are zero.

concentrated phytoplankton samples would not demonstrate optical activity. As is well known, amino acids and sugars have a 'handedness' or chirality and, therefore, when associated with the cells' pigments will induce a certain degree of optical activity (Houssier and Sauer, 1970). Also, Pospergelis (1969) measured the ratio of V/I for the Stokes vector of light reflected from green leaves and found the ratio to be of the order of a few percent but, for the low concentrations observed in the open oceans, measurement accuracies of one part in 10^4 are required.

1.6 Neutral points in the atmosphere and ocean

We have previously shown that, although incident sunlight is unpolarized, one of the important characteristics of the light field in the natural atmosphere and ocean is the polarization state, including the degree and plane of polarization. The polarization state of light contains valuable information about the optical properties of the atmosphere and ocean. On the other hand, in the angular distribution of the polarized light field, directions may exist where the light is actually unpolarized (or neutral) with a vanishing degree of polarization. These points in an angular distribution plot are called neutral points. The positions of neutral points are of great interest, as they are found to be sensitive indicators of various atmospheric optical properties, including atmospheric turbidity, air pollution, etc. (Bellver, 1987).

Measurements of neutral points were first made in a simple Rayleigh atmosphere. Early measurements included those by Arago (Barral, 1858), Babinet (1840), and Brewster (1842), who independently observed three different neutral points. All three neutral points are on the principal plane – the plane containing both the zenith and the Sun. The Arago point is normally 20° to 30° above the antisolar point, the Babinet point is approximately the same angular distance above the Sun, and the Brewster point is about 15° to 16° below the Sun. For a review of the observations of these three neutral points, readers are referred to Coulson (1988). The three neutral points have been well known for over a century and have been observed in separate measurements (e.g., Bellver, 1987; Coulson, 1983; Gal et al., 2001). As suggested by theory, a fourth neutral point should be in the principal plane that lies below the antisolar point, but was not observed until over a century later by Horvath et al. (2002) using measurements from a balloon-borne polarimeter.

From a theoretical perspective, a neutral point appears when a positive/negative polarization is exactly canceled by a negative/positive polarization. At the time the first three neutral points were observed, the origin of the opposite polarization state was not clear. Lord Rayleigh (1871) showed that Rayleigh scattering of light by atmospheric molecules introduced a large polarization at 90° to the incident beam, while the forward- and backward-scattered light (i.e., the scattered light at the solar and antisolar points) is unpolarized if only a single scattering is considered. This implied that two neutral points should be in these two directions, which differed from the observations. Later, Chandrasekhar (1951) using radiative-transfer theory showed that the opposite polarization state could be explained by multiple scattering of light in a Rayleigh atmosphere. According to radiative-transfer calculations, the neutral points at the solar point splits into two neutral points in